Earth Systems, Resources, and Sustainability, 2026, 1(1), 32–43

Scilight

Earth Systems, Resources, and Sustainability

Journal Homepage: https://www.sciltp.com/journals/esrs

Article

Stable Isotopic and Geospatial Approach for Evaluating the Frequent Occurrence of Cyclonic Events Over the Arabian Sea

Md. Arzoo Ansari, Jacob Noble* and Archana Deodhar

Isotope and Radiation Application Division, Bhabha Atomic Research Centre, Trombay, Mumbai 400085, India

* Correspondence: noblej@barc.gov.in

ABSTRACT

The frequency of cyclonic events has increased over the Arabian Sea in the recent past due to the influence of climate change on the Indian Ocean. This study integrates environmental isotopic tracers (δ^{18}O and δ^{2}H) and geospatial data to investigate the occurrence of Cyclone Nisarga during June, 2020, which impacted the Mumbai city, India. High frequency precipitation samples collected during the cyclone exhibited distinctly depleted and widely variable isotopic signatures (δ^{18}O: −15.9‰ to −0.2‰; δ^{2}H: −114.8‰ to 7.5‰; D-excess: 5.7‰ to 15.1‰), compared to the Indian Summer Monsoon (ISM), that is more enriched and having lower variability. These differences are attributed to the dynamic nature of moisture, isotopic fractionation due to organized convective condition and vapour recycling along the trajectory of the Cyclone Nisarga. The structural development and intensification of the cyclone were further examined using Sea Surface Temperature (SST), Outgoing Longwave Radiation (OLR), and wind circulation patterns derived from the HYSPLIT backward trajectory modelling. The elevated SST values and anthropogenic forcing are found to be the key factors responsible for the frequent cyclone genesis and its intensification over the Arabian Sea. The extremely low OLR values and distinct wind patterns are observed during the Cyclone Nisarga. Difference in wind dynamics and clouds patterns between tropical cyclones and the ISM highlight the unique atmospheric and hydro-meteorological processes responsible for the formation of the cyclone. The study offers valuable insights into the mechanisms of extreme rainfall events, aiding in improved forecasting, disaster mitigation, and climate resilience planning in the region.

ARTICLE INFO

History:

Received 14 October 2025
Revised 10 November 2025
Accepted 11 November 2025
Published: 20 November 2025

Keywords:

stable isotopes;
cyclone;
extreme events;
Arabian Sea;
sea surface temperature

Citation:

Ansari, M.A.; Noble J.; Deodhar A. Stable Isotopic and Geospatial Approach for Evaluating the Frequent Occurrence of Cyclonic Events Over the Arabian Sea. *Earth Systems, Resources, and Sustainability* **2026**, *1*(1), 32–43.

Research Highlights

- Hydro-meteorological processes responsible for the genesis and circulation pattern of the Cyclone Nisarga were evaluated using stable isotopes and geospatial data.
- Distinctly depleted and widely variable stable isotopic signature was observed during the cyclone.
- Isotopic characteristics and atmospheric processes were compared between the tropical cyclones and the Indian Summer Monsoon.
- Elevated sea surface temperature and anthropogenic forcings are the key factors responsible the frequent occurrence of tropical cyclones.

1. Introduction

The frequency and intensity of natural disasters (heavy rainfall events, cyclones and the resulting floods) in the tropical regions have been increased many-fold during the last two to three decades. This is largely due to the increased heating of the ocean surface resulting from anthropogenic drivers [1, 2]. Among these disasters, the tropical cyclones, which typically develop over the subtropical and tropical oceans, stand out as some of the most destructive events in the recent past. Tropical cyclones are low pressure systems having a warm core, dense cloud cover and gusty winds, causing torrential rainfall. These cyclones generally form when the wind speed exceeds 18 m/s over the ocean and subsequently migrate to higher latitudes, till they landfall over the continental areas or cooler sea waters. While the study on genesis of tropical cyclone remains an area of ongoing research, several critical factors are known to contribute for the generation of cyclone. These include: elevated Sea Surface Temperature (SST) [3, 4], enhanced low-level cyclonic vorticity [5], reduced vertical wind shear in the environment [6], high atmospheric humidity near the equator and deflection caused by the Coriolis force, which promotes the rotational motion.

Globally, around 80 tropical cyclones form annually, predominantly in summer or early autumn [7]. Cyclones typically develop over the Northern Indian Ocean (NIO), during April–June (pre-monsoon) and October–December (post-monsoon) months. They frequently occur in the Bay of Bengal (BoB), while, only one or two cyclones typically occur each year in the Arabian Sea [8]. Despite the consistently high SST in the NIO during the Indian Summer Monsoon (July–August), cyclogenesis is notably suppressed because of the strong vertical wind shear caused by intense atmospheric monsoonal circulation [9]. The intensity of tropical cyclones over the Arabian Sea has shown a marked increase in the last two to three decades [2, 10, 11]. This intensification has been linked to factors such as reduced vertical wind shear and changes in atmospheric circulation, potentially driven by increased anthropogenic aerosol emissions over the NIO [1, 2, 6, 12].

A notable rise in cyclonic activities observed in the recent years over the Arabian Sea, include: (i) The Cyclone Nilofar developed during 25–30 October, 2014, with wind speeds more than 46 m/s, caused widespread damage [13]. Again, in 2015, Cyclones Chapala and Megh made landfall in Yemen, bringing very strong winds, resulting in significant casualties and displacements [14] and after two years, i.e., in 2017, Cyclone Ockhi cause destruction in South India, Maharashtra, Gujarat, The Maldives, Sri Lanka and Lakshadweep. This increase in cyclone frequency is because of anthropogenic forcing, weakening of winter monsoon circulation, reduced wind shear, and rising SST [15].

Furthermore, the Indian Ocean, particularly its western region, has shown anomalous warming compared to the other part, since the early 20th century. The SST of the Western Indian Ocean during the summer month had shown a marked rise from $\sim$26.5 °C to $\sim$28.0 °C, an anomalous increase of approximately 1.2 °C, between 1901 and 2012 [16]. This warming, which is greater than the rest of the tropical Indian Ocean, has altered the SST gradients, consequently disrupted the monsoonal circulation and rainfall patterns of Asian regions.

The applications of stable water isotopes, oxygen (δ^{18}O) and hydrogen (δ^{2}H) in precipitation help in understanding the hydrological and atmospheric dynamics of tropical cyclones. These isotopes of precipitation are sensitive to complex atmospheric processes such as convection, advection, condensation, evaporation, vapour interactions, moisture transport pathways, moisture recycling etc. [17–20], therefore, the isotopic characteristics of precipitation during the cyclone can be used to decipher the atmospheric factors that are most dominant during the event.

Stable isotope ratios (δ^{18}O and δ^{2}H) have been widely used for over six decades to study the precipitation processes, moisture transport pathways, and source regions [21–27]. These isotopic signatures are shaped by a wide range of hydro-meteorological factors, including temperature, humidity, amount of precipitation, convective strength, latitude, altitude, and rain-vapor interactions [28–32]. Synoptic weather systems, particularly the cyclones, can cause pronounced changes in isotopic composition [19, 31, 33–35]. Ref. [36] reported rapid isotopic depletion during the Hurricanes Otto, Irma, and Maria in the Mesoamerican region. Similarly, Ref. [37] also documented isotopic changes in typhoon rains in Southeast China, linking them to large-scale convection and moisture recycling, Ref. [31] discussed a distinctly depleted isotopic content during the Cyclone Ockhi and linked it with convective condition and moisture recycling. These studies highlight the utility of stable isotopes in understanding the structure and evolution of cyclones.

Cyclogenesis is driven by a complex set of processes (low wind shear, Coriolis force, etc.) with high SST being a key factor [38, 39]. A threshold of 26.5 °C is considered as essential SST for the genesis of tropical cyclones [1, 2, 40–42]. At SST above 26.5 °C, the energy for cyclogenesis is predominantly supplied by latent heat fluxes from the sea surface, which provide the necessary fuel for deep convection [3]. In regions with SST below 26.5 °C, baroclinic instability may compensate for the lack of SST-driven energy [43].

Cyclones are a form of deep tropical convection, which drives the atmospheric heat engine known as the Hadley circulation [44]. Convective instability and SST are tightly coupled, with deep convection being rare at SST below 26 °C, but intensifies as SST increases [45]. The deep tropical convection is commonly assessed using Outgoing Longwave Radiation (OLR), which quantifies the thermal radiation emitted by the earth. Lower OLR values are indicative of stronger, more extensive convection [46].

The present study focuses on Mumbai, located on the windward side of the Western Ghats along the western coastline of India. The city receives moderate to high rainfall due to the orographic lifting of monsoon winds, with

an annual average of ∼2422 mm. Mumbai experiences the Indian Summer Monsoon from mid-June to September, with temperature ranging from 16.3 °C to 32.2 °C. The city has experienced several extreme events in the recent past, Cyclone Ockhi in 2017 was the first cyclone to make a landfall in Mumbai in the last 70 years, followed by two other cyclones, Cyclone Nisarga and Tauktae in 2020 and 2021, respectively and an unprecedented rainfall on July 26, 2005, when 944 mm fell in 24 hrs—the highest recorded daily rainfall in Mumbai. Cyclone Nisarga, which struck on June 3, 2020, was the most intense tropical cyclone to affect the Maharashtra State in June (i.e., before the onset of monsoon) since 1891, with wind speeds reaching 110 km/h and a recorded rainfall of 72.5 mm during the event. The cyclone made landfall at 95 km south of Mumbai, before weakening and dissipating in the next day.

With this background, the present study aims to (i) investigate the isotopic evolution of precipitation during the Cyclone Nisarga, which occurred over the Arabian Sea during June 2–3, 2020; (ii) compare the isotopic characteristics of cyclonic rains with those of Indian Summer Monsoon and (iii) to understand the atmospheric and hydrometeorological processes contributing to the cyclogenesis and precipitation characteristics during the tropical cyclones.

By integrating stable isotope hydrology with geospatial and meteorological data analyses, the present study enhances our understanding of tropical cyclones occurring over the Arabian Sea and their evolving nature in response to climate variability and anthropogenic influences.

2. Methods

2.1. Rainwater Sampling and Isotopic Analysis

High frequency rainwater sampling was conducted during the Cyclone Nisarga (June 2–3, 2020) to investigate the isotopic characteristics associated with cyclonic precipitation. To minimize the isotopic fractionation due to the evaporation, a specially designed rainwater sampling device made up of polyethylene container with funnel and a narrow tube fixed at the top of the device to create pressure equilibrium, was employed following the protocol outlined in Ref. [47]. The sampling station was located along the coastal region of Mumbai City at an elevation of approximately 10–25 m amsl (Figure 1). Rainwater samples were collected at 1–3 hr intervals throughout the duration of the cyclone in 20 ml polythene bottles, tightly capped and sealed without air bubble and stored in a cool environment to prevent evaporation and exchange with air. For comparative analysis, additional samples were collected during non-cyclonic summer monsoon events to evaluate the isotopic differences between cyclonic and non-cyclonic rainfall. Stable isotopes (δ^{18}O and δ^{2}H) were analyzed using a continuous flow Isotope Ratio Mass Spectrometer (IRMS, model-Isoprime-100). δ^{18}O values were determined using the CO_2–H_2O equilibration method [48], while δ^{2}H was measured via high-temperature pyrolysis using an elemental analyzer attached to the IRMS. The isotopic results are reported in standard delta notation (δ) relative to the Vienna Standard Mean Ocean Water (V-SMOW) as [49]:

$$\delta^{2}\text{H}(\text{or } \delta^{18}\text{O}) = \left(\frac{R_{\text{sample}} - R_{\text{standard}}}{R_{\text{standard}}} \right) \times 10^{3} \qquad (1)$$

where R_{sample} is the isotope ratio (^{2}H/^{1}H, ^{18}O/^{16}O) of a sample and R_{standard} is the corresponding ratio of the standard [50]. The δ-values are expressed in permil (‰). The measurement precision was $\pm$0.5‰ for δ^{2}H and $\pm$0.2‰ for δ^{18}O at the 2σ level.

For assessing the origin, structure and intensity of Cyclone Nisarga, geospatial datasets of Sea Surface Temperature (SST) and Outgoing Longwave Radiation (OLR) were analyzed over the region spanning 0°–30°N and 50°–100°E. SST and OLR data were downloaded from the NOAA satellite-based reanalysis datasets [51] archived at the National Center for Atmospheric Research (NCAR) (www.esrl.noaa.gov/psd/data/gridded/reanalysis) (accessed on 15 September 2025).

To determine the source regions supplying moisture to the precipitation during the cyclone, air mass backward trajectories were computed using the Hybrid Single-Particle Lagrangian Integrated Trajectory (HYSPLIT v4.0) model developed by NOAA [52]. Trajectories were evaluated at altitudes of 5500 m above ground level (agl), representing typical cloud heights during tropical cyclonic systems [53]. The modeled trajectories were then compared with isotopic data to infer the moisture transport pathways and potential sources.

3. Results and Discussion

3.1. Stable Isotopes (δ^{18}O and δ^{2}H)

The δ^{18}O and δ^{2}H of precipitation in Mumbai exhibits distinct differences between cyclonic and non-cyclonic events. During the Indian Summer Monsoon (ISM) period under non-cyclone conditions, δ^{18}O and δ^{2}H values ranges from -2.5 to 0.9‰ and -7 to 15‰, respectively, with mean values of -0.5 ± 0.8‰ and 6.2 ± 4.2‰ (Figure 2a). In contrast, the precipitation associated with Cyclone Nisarga was significantly more depleted and found to be widely varied, with δ^{18}O ranging from -15.9‰ to -0.2‰ and δ^{2}H from -114.8‰ to 7.5‰, with mean values of -6.4 ± 5.2‰ for δ^{18}O and -47.1 ± 45.1‰ for δ^{2}H. During the torrential rainfall event over Mumbai on 26 July, 2005 which recorded 944 mm in 24 hrs, exhibited δ^{18}O values ranging from -2.2‰ to -0.9‰ (mean: -1.3‰), aligning closely with the ISM rains in Mumbai [31]. These observations indicate that the rainfall during Cyclone Nisarga was markedly more depleted in heavy isotopes than the regular monsoon precipitation (Figure 2a).

To further investigate these variations, δ^{18}O values were plotted against δ^{2}H along with the Global Meteoric Water Line (GMWL) discussed in Ref. [49]:

$$\delta^{2}\text{H} = 8\delta^{18}\text{O} + 10 \qquad (2)$$

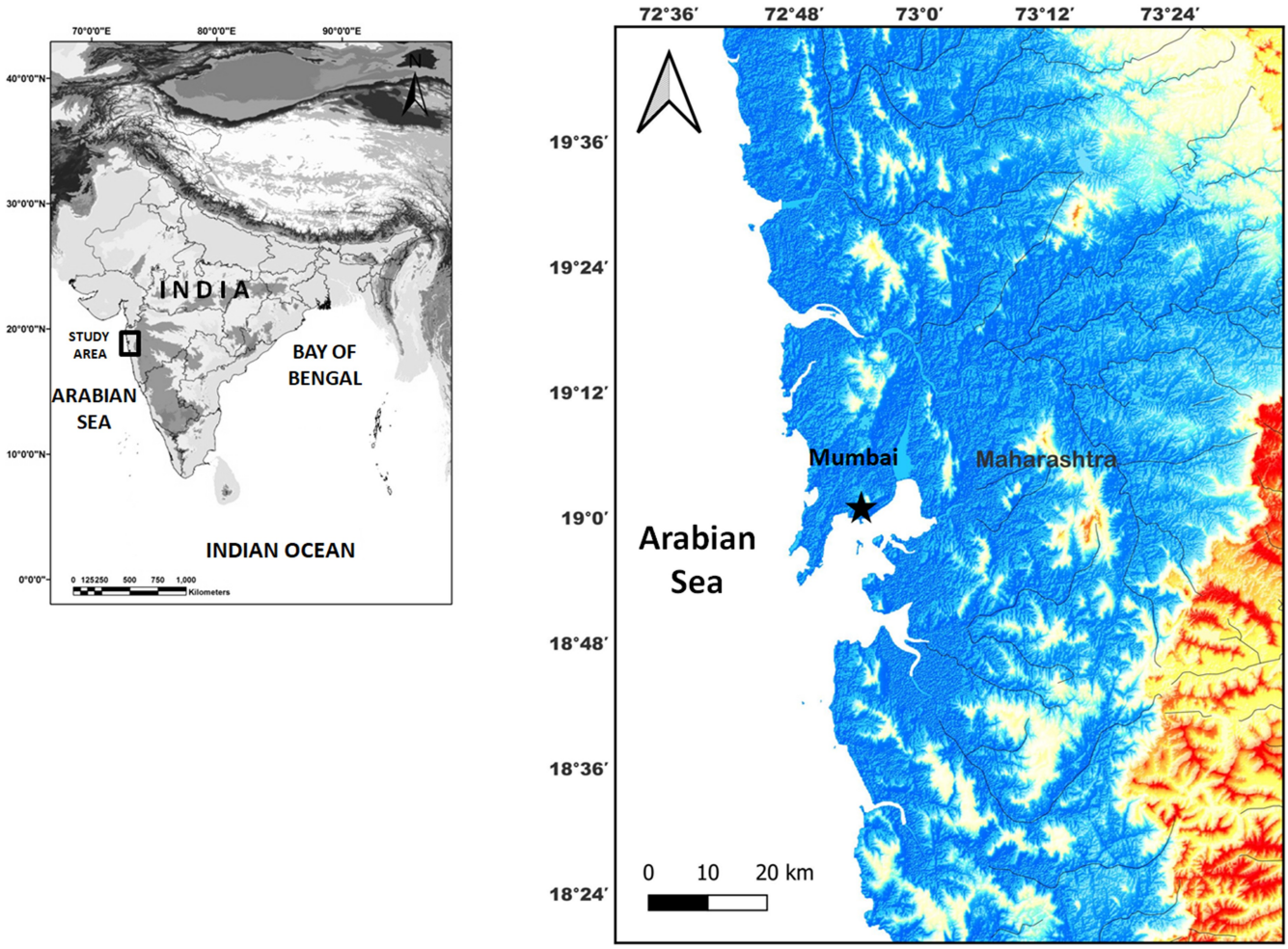

Figure 1. Map showing the sampling location during the Cyclone Nisarga.

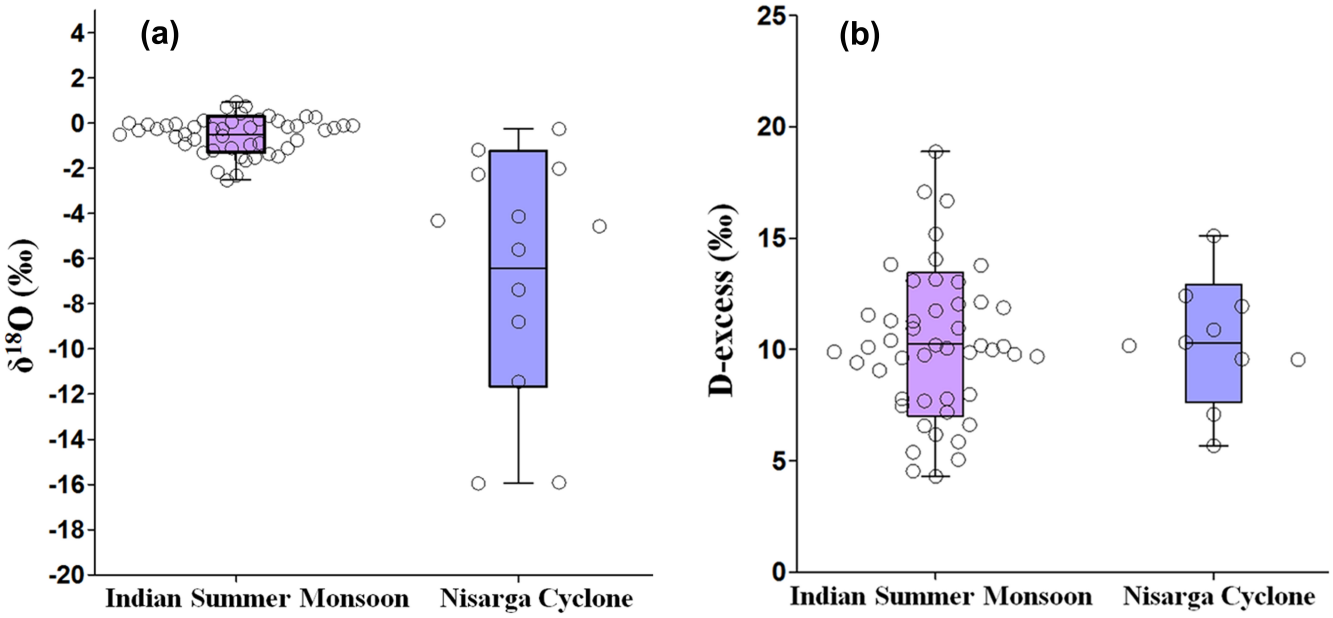

Figure 2. (**a**) δ^{18}O and (**b**) D-excess variability during Cyclone Nisarga and Indian Summer Monsoon.

Additionally, the Local Meteoric Water Line (LMWL) for Mumbai, Ref. [31] is:

$$\delta^{2}\mathrm{H} = (8.9 \pm 0.5)\delta^{18}\mathrm{O} + (10.5 \pm 0.9) \quad (3)$$

In the δ^{18}O–δ^{2}H plot (Figure 3), the precipitation samples during the ISM falls in one cluster along the GMWL and do not show wide variations, indicating prevalence of equilibrium fractionation processes. However, the precipitation samples of Cyclone Nisarga are widely distributed along the GMWL, with significantly depleted values during the peak cyclone to less depleted and same as that of the ISM during the dissipation phase of the cyclone (Figure 3). This pattern suggests the dominance of large-scale convective processes during the cyclone, leading to strong isotopic fractionation and removal of heavier isotopes through progressive condensation and rainout. Similar depletion trends during the tropical cyclones have been reported in previous studies [18, 54], where the isotopic signature reflects the widespread condensation processes and intense updraft within the cyclone. The depletion is often more pronounced in δ^{2}H due to stronger rainout effects on hydrogen isotopes. Such isotopic depletion may extend several kilometers from the core to its periphery of the cyclone [55] and typically, the depletion becomes more pronounced at the centre of the cyclone [56].

3.2. Deuterium Excess (D-excess)

The deuterium excess (D-excess), defined in Ref. [57] as:

$$\text{D-excess} = \delta^{2}\text{H} - 8 \times \delta^{18}\text{O} \quad (4)$$

D-excess is a crucial metric used to assess the effect of kinetic fractionation under non-equilibrium conditions, viz., the evaporation of water vapour above the sea surface [27, 58]. Also, it provides insight into the thermal conditions and vapor balance during the formation of air masses over both the sea and land. D-excess is often employed to infer the environmental conditions at the moisture source regions and it is controlled by RH, air temperature, SST, and isotopic composition of water at the sea surface. D-excess also retains the climatic signature under which precipitation occurs, reflecting the factors like relative humidity (RH), air temperature, supersaturated conditions and moisture transport pathways [59, 60]. Additionally, it can help to track recycling of moisture over both the ocean and the continents [61].

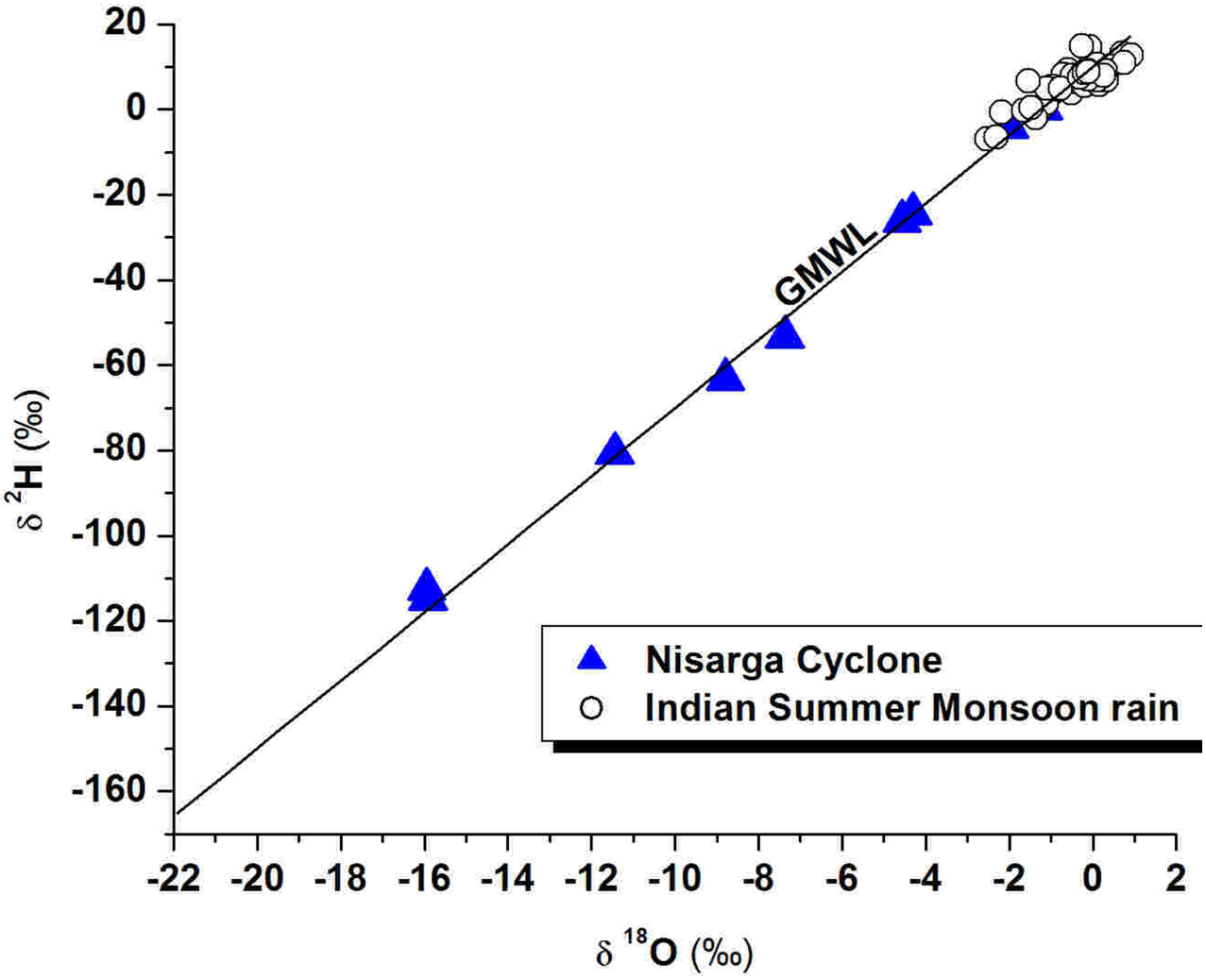

Figure 3. δ^{18}O and δ^{2}H plot showing the variations in stable isotopic composition of precipitation during the Cyclone Nisarga and Indian Summer Monsoon.

D-excess generally shows an inverse relationship with RH, because of the fractionation resulting from the molecular diffusion at the air–sea interface. The diffusion process is influenced by air temperature and wind dynamics [62]. Additionally, D-excess shows positive correlation with SST, because of the kinetic and equilibrium fractionation occurring during the phase transitions [63].

Under dry climate, the degree of kinetic fractionation increases due to elevated evaporation rates. As a result, the vapor formed during evaporation tends to have higher D-excess while the residual water exhibits lower D-excess values. Rain occurring from such vapour clouds also shows high d-excess [32, 50]. However, in the case of low rainfall, the sub-cloud evaporation causes reduction in the D-excess values [60, 64]. Therefore, the D-excess can be used as a powerful proxy to decipher the meteorological conditions in the moisture source regions that causing rain during the cyclonic and non-cyclonic events [35, 65, 66].

In the present study, the D-excess values of ISM precipitation ranged from 4.3‰ to 18.8‰ with a mean of 10.2 $\pm$ 3.2‰, closely matching with the global average value of 10‰ (Figure 2b). Lower value in some samples suggests sub-cloud evaporation of the falling rain drops during light rainfall events [67].

The D-excess values of precipitation during the Cyclone Nisarga, ranged from 5.7‰ to 15.1‰, with an average of 10.2 $\pm$ 2.6‰, again align with the global mean value (10‰). However, several samples exhibit higher values than the average D-excess, potentially reflecting the isotopic fractionation during the transport of moisture from the sea to the continental location of Mumbai. The elevated D-excess could be attributed to the processes such as evaporation under low RH, condensation, and large-scale atmospheric circulation associated with the cyclone [63]. These finding provide insight into the role of D-excess as a proxy for understanding the hydro-meteorological and oceanic conditions influencing the moisture transport and precipitation during both cyclonic and non-cyclonic events.

3.3. Temporal Variations of $\delta^{18}O$ and D-excess during the Cyclone Nisarga

The temporal evolution of δ^{18}O and D-excess during the Cyclone Nisarga reveals the changes in moisture dynamics and atmospheric and hydrological processes throughout the event. Significantly large fluctuations were observed in hourly data of both the parameters (δ^{18}O and D-excess) (Figure 4a, b), reflecting the variation in moisture sources and hydro-meteorological conditions during the lifecycle of the cyclone. During the onset of cyclone, the δ^{18}O was approximately ~-4‰ and D-excess was $\sim$10‰. However, the δ^{18}O become highly depleted (-15.9‰), and the D-excess dropped to a lower value of $\sim$5.7‰ during the peak phase of the cyclone. Interestingly, the δ^{18}O become relatively enriched (-2‰) and D-excess increased to a maximum ($\sim$15.1‰) during the dissipation phase. This pattern of isotopic evolution may be because of the large-scale moisture circulation, RH, evaporation and moisture recycling during the different phases of cyclone. Low D-excess during the peak phase coincided with high RH and wind speeds, leading to reduced kinetic fractionation. The subsequent increase in D-excess during the dissipation phase likely resulted from enhanced continental moisture recycling and reduced RH. The isotopic enrichment observed during the post-peak period may also reflect reduced convective activity and changes in moisture source regions. Such temporal variations align with previous studies suggesting that the isotopic content of rainfall is sensitive to changes in cyclone dynamics, moisture transport pathways, and rainout processes [31, 64].

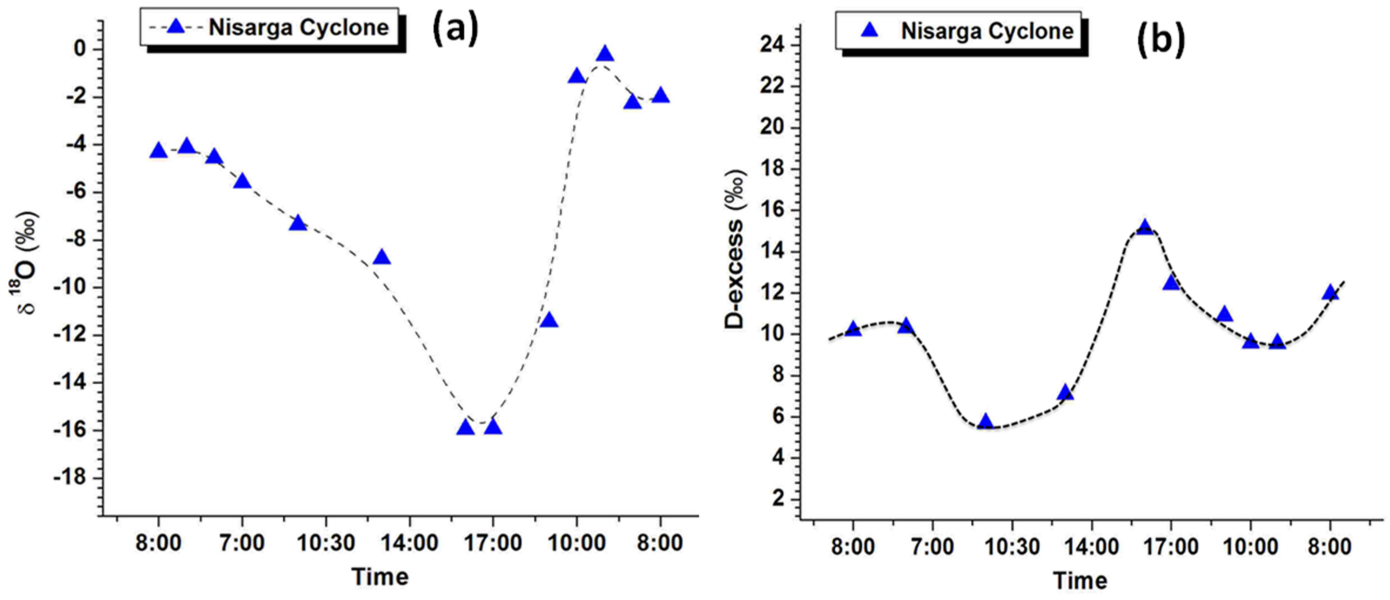

Figure 4. Time series plots of (**a**) δ^{18}O & (**b**) D-excess during the Cyclone Nisarga.

3.4. Comparison of Isotopic Characteristics of Cyclone Nisarga with other Tropical Cyclones

A comparative study was conducted between the isotopic characteristics of tropical cyclone formed in the Indian Ocean and those from the Pacific and the Atlantic (Figure 5). These comparisons include: Cyclone Ockhi (Arabian Sea, December 2017) [31], Cyclone Phailin (Bay of Bengal, 2013) [23], Typhoon Shanshan (Western Pacific Ocean, 2006) [55], Cyclone Ita (Southwest Pacific Ocean, 2014) [68], Cyclone Sandy (North Atlantic Ocean, 2012) [69], and Cyclone Irma (Atlantic Ocean, 2017) [36].

The isotopic signature of Cyclone Nisarga is notably depleted, exhibiting significant variation with that of the Cyclone Ockhi, both occurred in the Arabian Sea. However, the isotopic evolution of Nisarga aligns more closely with the Cyclone Irma from the Atlantic. Similarly, the isotopic values of Cyclone Nisarga share similarities with Cyclone Phailin from the Bay of Bengal, although with larger variability. These observations suggest that the hydrometeorological processes governing the genesis of Cyclone Nisarga are similar to those of Cyclone Irma. In contrast, Typhoon Shanshan, Cyclone Ita and Cyclone Sandy show markedly different isotopic signatures (i.e., more depleted) compared to those observed in the Indian Ocean (Cyclones Ockhi and Phailin) and from the Atlantic (Cyclone Irma).

3.5. Role of Sea Surface Temperature (SST) in the Formation and Intensification of Cyclone Nisarga

Tropical cyclones are primarily driven by high SST and strong mid-level vortices [70]. Previous studies established a linear relationship between the SST and the maximum potential intensity of tropical cyclones [71]. Therefore, the present study analyzes the SST over the Arabian Sea to better understand the cyclogenesis.

The analysis of mean SST data before the formation of Cyclone Nisarga revealed that the SST over the Arabian Sea exceeded 30 °C, for up to 10 days prior to the cyclone (Figure 6), in comparison to the long-term average of 28 °C [72]. However, the SST decreased slightly, but remained generally high during the active period of the cyclone. Long-term SST data (1917–2017) also show that the SST prior to the Cyclone Nisarga were significantly elevated, suggesting a substantial contribution of moisture and energy input that likely intensified the cyclone. It has been shown that a 0.5 °C rise in SST can boost the intensity of a cyclone up to 10% [73]. The high SST anomaly (ranging from 0.4 °C to 1.3 °C above the long-term average) observed over the Arabian Sea likely provided the necessary energy for latent heat flux, enabling the intensification of the cyclone [31]. Such high positive SST anomalies may also be linked to climate change, as anthropogenic activities have caused significant heating of the ocean surface over the past five decades [6, 15], potentially increasing the prevalence of cyclonic storms in the Indian Ocean.

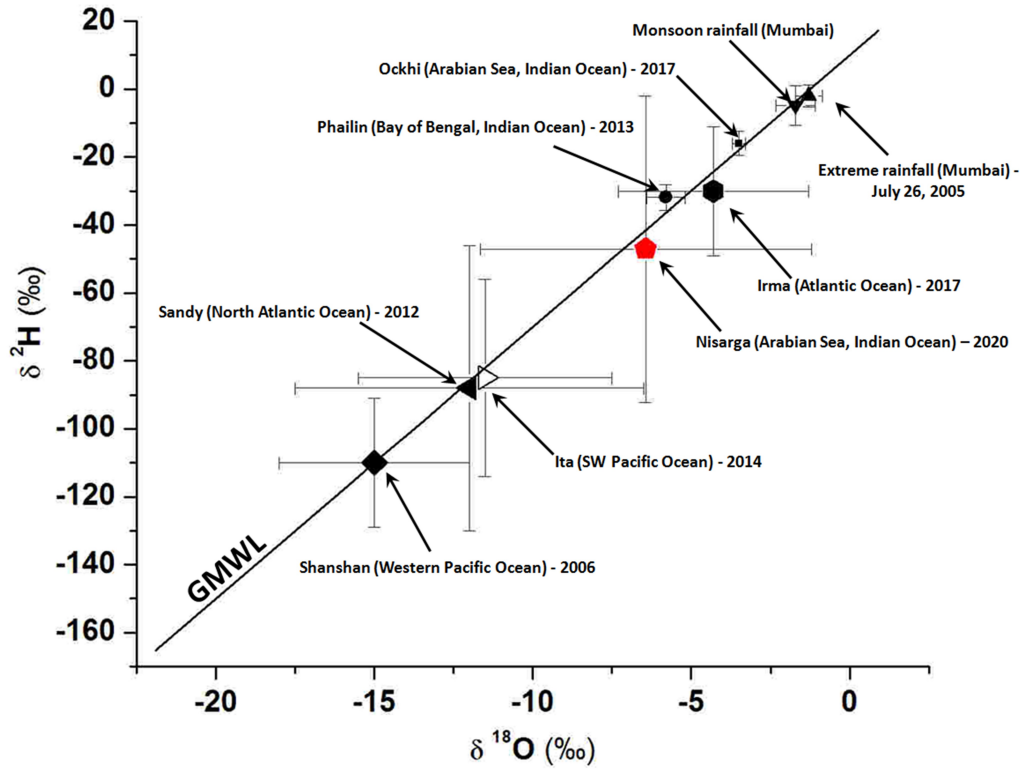

Figure 5. Isotopic comparison of major tropical cyclones occured in different oceans with those of Cyclone Nisarga, at Mumbai.

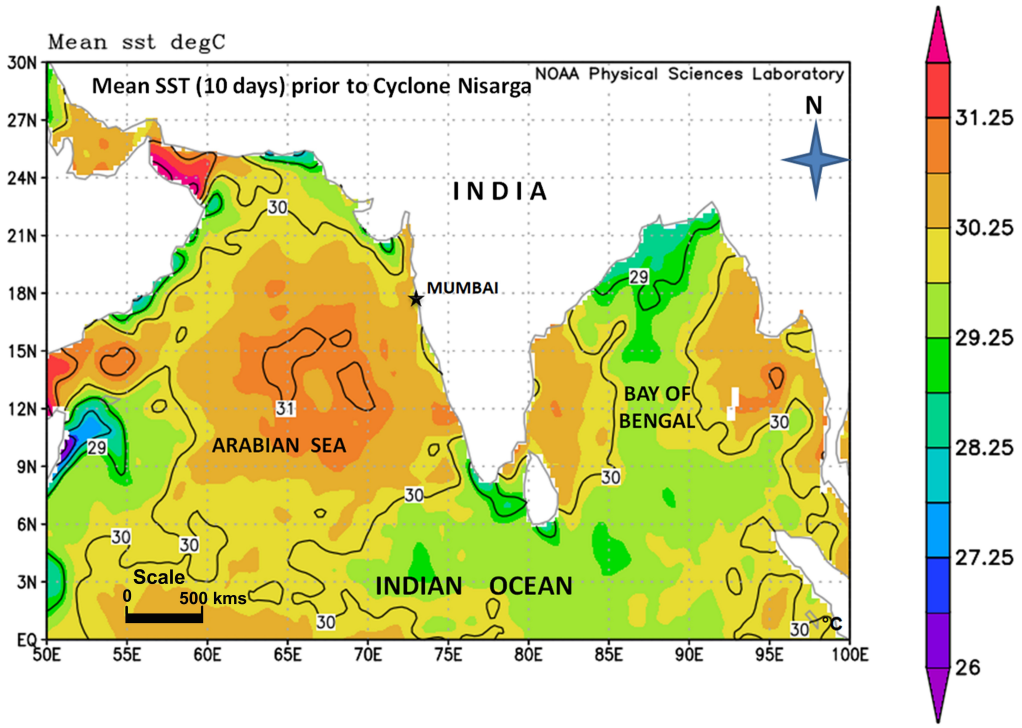

Figure 6. Spatial variability of mean SST prior to the Cyclone Nisarga.

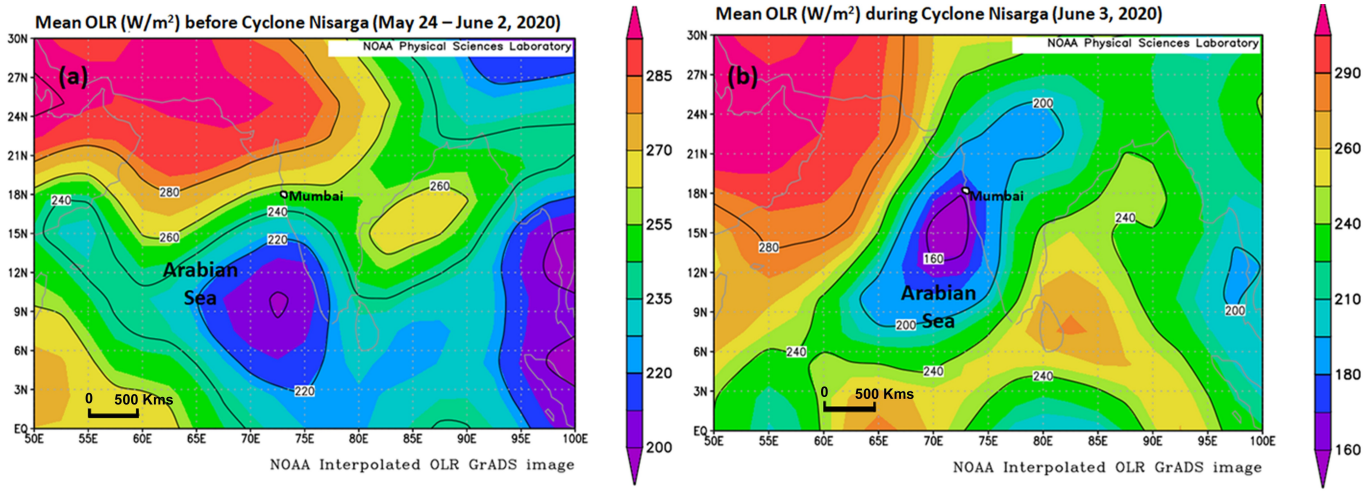

Figure 7. Spatial variability of mean OLR (W/m^2) prior to and during the Cyclone Nisarga.

3.6. Correlation between Outgoing Longwave Radiation (OLR) and the Development of Cyclone Nisarga

The convection processes associated with the Cyclone Nisarga was studied using the OLR data obtained from NOAA with a spatial resolution of 2.5°× 2.5° [51]. The results show that the areas with SST exceeding 28 °C were characterized by OLR values of less than 240 W/m^2, reflecting large-scale deep convection [29, 74]. Prior to Cyclone Nisarga, the OLR values over the Arabian Sea were less than 220 W/m^2, and by June 3, 2020 (the peak period of the cyclone), OLR values dropped below 160 W/m^2 over the central Arabian Sea near Mumbai and Goa. This sharp decrease in OLR corresponds to a strong, organized deep convection centered around the cyclone, further corroborating the link between high SST and intense tropical convection.

The spatial distribution of SST and OLR data indicates a close correlation between these two parameters, with regions having SST over 28 °C corresponding to lower OLR values (Figure 7). This suggests that the high sea surface temperature is a critical factor in triggering the onset of deep convection, which subsequently intensifies the cyclone. The pattern of OLR before and during the Cyclone Nisarga further demonstrates that the intensified convection follows the path of the cyclone, confirming the significance of understanding deep convection and its development.

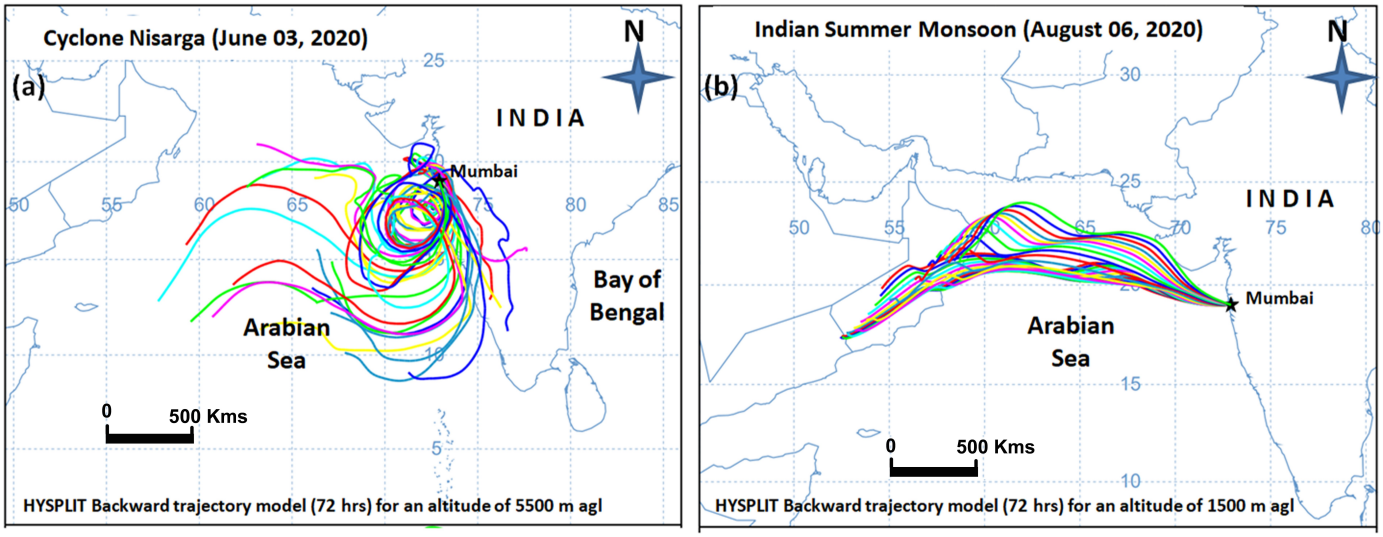

Figure 8. HYSPLIT backward trajectory model (**a**) 72 hrs prior to the Cyclone Nisarga (June 03, 2020) for an altitude of 5500 m above ground level (agl); (**b**) 72 hrs prior to the rainfall day during Indian Summer Monsoon (06 August 2020) for an altitude of 1500 m agl.

3.7. Atmospheric Circulation Pattern and their Connection to Stable Isotopic Variability

HYSPLIT modelling was conducted using the NOAA/NCEP reanalysis data to identify the moisture sources region contributing to the precipitation in Mumbai during the Cyclone Nisarga and the Indian Summer Monsoon (ISM), and also to explain the stable isotope variability in precipitation. Backward trajectory analyses were conducted for two key dates: June 3, 2020 (Cyclone Nisarga), and August 6, 2020 (typical ISM rainfall event). Trajectories were calculated at 1-hr intervals over a 72-hr period prior to the rainfall event at a height of 5500 m agl (Cyclone Nisarga) and 1500 m agl (ISM) (Figure 8a). During the Cyclone Nisarga, the wind trajectories revealed a prominent cyclonic circulation over the Arabian Sea. These air masses originated over the Arabian Sea near the sea level and ascended to higher altitudes (∼5500 m agl), indicating strong convective uplift. The circular wind pattern facilitated significant vertical movement of moisture from the sea surface to the upper atmosphere, where high-altitude clouds were formed and precipitated over the sampling location. This uplift, combined with prolonged moisture transport and intensive convective activity, led to the pronounced isotopic depletion (more negative δ^{18}O values). The strong isotopic fractionation observed can be attributed to the processes such as rainout during the ascent and sub-cloud interactions. During the tropical cyclone, the cloud bases were observed between 573 and 713 m agl and cloud tops extending to much greater heights [31]. The prevalence of high-altitude clouds likely contributed to the observed depleted isotopic signatures during the cyclone.

In contrast, the wind pattern during the ISM event displayed predominantly horizontal movement with limited vertical ascent (Figure 8b). For this analysis, the backward trajectories were calculated at 1500 m agl, as more than 90% of the monsoonal rainfall in the region occurs at or below this altitude [31]. It is seen that these trajectories originated near the Western region of the Arabian Sea.

During this transit, the air masses picked up moisture from the ocean, but due to relatively limited vertical uplift, the isotopic fractionation processes were less intense. As a result, the δ^{18}O values were less depleted, than those observed during the cyclone. The lower altitude of the cloud formation and horizontal nature of the airflow reduced the extent of rainout and minimized the sub-cloud interactions. This distinction is consistent with the previous findings suggesting that the vertically ascending air masses are associated with greater δ^{18}O depletion, while, horizontal or descending trajectories result in less isotopic alteration [31, 75, 76].

Overall, the trajectory analysis clearly demonstrates that the atmospheric circulation patterns strongly influence the isotopic composition of precipitation. The more depleted δ^{18}O values observed during the Cyclone Nisarga is because of the enhanced isotopic fractionation due to the intense convective activity and the resulting vertical transport of moisture. In contrast, the less depleted isotopic signature observed during the typical ISM events is associated with the low-level, horizontally moving air masses, highlighting the distinct hydro-meteorological and moisture transport mechanisms associated with different rainfall systems over the Arabian Sea.

4. Conclusions

This study presents a novel integration of stable isotopic analysis and geospatial data to evaluate the genesis and characterization of Cyclone Nisarga occurred during June 03, 2020 over the Arabian Sea. The distinctly

depleted and widely variable isotopic signature of the precipitation samples collected during the cyclone in Mumbai, when compared to the Indian Summer Monsoon and other extreme rainfall events, highlight the dynamics of moisture processes driving such cyclonic systems. The elevated SST values and anthropogenic forcing are the key factors responsible for the frequent cyclone genesis and its intensification over the Arabian Sea. Extremely low OLR value with distinct wind patterns and cloud structure was found during the cyclone and is sharply contrasted with those observed during the monsoonal events.

The findings of the present study provide valuable insights into the mechanisms underlying the extreme events. This knowledge is crucial for hydrologists and climatologists in developing more effective disaster management strategies, particularly in the context of rising frequency and intensity of tropical cyclones due to climate change.

Author Contributions

M.A.A.: Conceptualization; Literature review; Data curation; Formal analysis; Plotting; Interpretation; Visualization; Writing original draft. J.N.: Conceptualization; Literature review; Interpretation; Modelling; Validation; Writing-review & editing. A.D.: Analysis; Review; Interpretation; Supervision. All authors have read and agreed to the published version of the manuscript.

Funding

This research received no external funding.

Institutional Review Board Statement

Not applicable.

Informed Consent Statement

Not applicable.

Data Availability Statement

All data used in this work are presented in the paper.

Acknowledgments

The authors express their gratitude to Dr. R. Acharya, Head, IRAD for his encouragement and support. They also extend thanks to Mr. G.N. Mendhekar and Mr. S.N. Kamble, IRAD, BARC for their valuable assistance during the investigation.

Conflicts of Interest

The authors declare that they have no known competing financial interests or personal relationships that could have appeared to influence the work reported in this paper.

Use of AI and AI-assisted Technologies

The authors have not used any AI tools for the preparation of the manuscript.

References

1. Bhatia, K.T.; Vecchi, G.A.; Knutson, T.R.; et al. Recent increases in tropical cyclone intensification rates. *Nat. Commun.* **2019**, *10*, 635. https://doi.org/10.1038/s41467-019-08471-z
2. Wu, D.; Ju, X.; Sun, J.; et al. Escalation of tropical cyclone impacts on the northwestern Bay of Bengal over the past decade. *Clim. Dyn.* **2024**, *62*, 5645–5662. https://doi.org/10.1007/s00382-024-07252-9
3. Defforge, C.L.; Merlis, T.M. Observed warming trend in sea surface temperature at tropical cyclone genesis. *Geophys. Res. Lett.* **2017**, *44*, 1034–1040. https://doi.org/10.1002/2016GL071045
4. Xu, M.; Wang, X.; Sun, L.; et al. Composited sea surface responses to tropical cyclones in the Bay of Bengal during 2003–2020. *Mar. Environ. Res.* **2024**, *202*, 106779. https://doi.org/10.1016/j.marenvres.2024.106779
5. Gray, W.M. Global view of the origin of tropical disturbances and storms. *Mon. Weather Rev.* **1968**, *96*, 669–700.
6. Evan, A.T.; Camargo, S.J. A climatology of Arabian Sea cyclonic storms. *J. Clim.* **2011**, *24*, 140–158.
7. Sobel, A.H.; Wing, A.A.; Camargo, S.J.; et al. Tropical cyclone frequency. *Earth's Future* **2021**, *9*, e2021EF002275. https://doi.org/10.1029/2021EF002275
8. Singh, V.K.; Roxy, M.K. A review of ocean–atmosphere interactions during tropical cyclones in the North Indian Ocean. *Earth-Sci. Rev.* **2022**, *226*, 103967. https://doi.org/10.1016/j.earscirev.2022.103967
9. Li, Z.; Yu, W.; Li, T.; et al. Bimodal character of cyclone climatology in Bay of Bengal modulated by monsoon seasonal cycle. *J. Clim.* **2013**, *26*, 1033-1046.
10. Singh, O.P.; Kahn, A.; Rahman, S. Has the frequency of intense tropical cyclones increased in the North Indian Ocean? *Curr. Sci.* **2001**, *80*, 575–580.
11. Vinodhkumar, B.; Busireddy, N.K.R.; Ankur, K.; et al. On occurrence of rapid intensification and rainfall changes in tropical cyclones over the North Indian Ocean. *Int. J. Climatol.* **2021**, *42*, 714–726. https://doi.org/10.1002/joc.7268
12. Cheng, L.; Abraham, J.; Hausfather, Z.; et al. How fast are the oceans warming? *Science* **2019**, *363*, 128–129. https://doi.org/10.1126/science.aav7619
13. WMO. *Tropical Cyclone Operational Plan for the Bay of Bengal and Arabian Sea WMO/TD-84*. World Meteorological Organization, 2015. https://www.wmo.int/pages/prog/www/tcp/documents/TCP-21Edition2015_final.pdf
14. Kruk, M.C. Tropical cyclones, North Indian Ocean. *Bull. Am. Meteorol. Soc.* **2016**, *97*, 114–115.
15. Murakami, H.; Vecchi, G.A.; Underwood, S. Increasing frequency of extremely severe cyclonic storms over the Arabian Sea. *Nat. Clim. Change* **2017**, *7*, 885–889. https://doi.org/10.1038/s41558-017-0008-6
16. Roxy, M.K.; Ritika, K.; Terray, P.; et al. The curious case of Indian Ocean Warming. *J. Clim.* **2014**, *27*, 8501–8509. https://doi.org/10.1175/JCLI-D-14-00471.1
17. Ansari, M.A.; Noble, J.; Deodhar, A.; et al. Atmospheric factors controlling the stable isotopes (δ^{18}O and δ^{18}O) of the Indian summer monsoon precipitation in a drying region of Eastern India. *J. Hydrol.* **2020**, *584*, 124636. https://doi.org/10.1016/j.jhydrol.2020.124636
18. Sun, C.; Tian, L.; Shanahan, T.M.; et al. Isotopic variability in tropical cyclone precipitation is controlled by Rayleigh distillation and cloud microphysics. *Commun. Earth Environ.* **2022**, *3*, 50.
19. Murillo, R.S.; Herrera, D.A.; Farrick, K.K.; et al. Stable isotope tempestology of tropical cyclones across the North Atlantic and Eastern Pacific Ocean basins. *Ann. N. Y. Acad. Sci.* **2024**, *1543*, 145-165. https://doi.org/10.1111/nyas.15274
20. Lekshmy, P.R.; Chirsty, A.A.; Krishnadas, S.; et al. Anomalous oceanic moisture supply conceals expected stable water

isotopic depletion during monsoon extreme rain events in Kerala, India. *Sci. Total Environ.* **2025**, *988*, 179758. https://doi.org/10.1016/j.scitotenv.2025.179758

21. Kumar, B.; Rai, S.P.; Kumar, U.S.; et al. Isotopic characteristics of Indian precipitation. *Water Resour. Res.* **2010**, *46*, W12548. https://doi.org/10.1029/2009WR008532
22. Aggarwal, P.K.; Romatschke, U.; Araguas-Araguas, L.; et al. Proportions of convective and stratiform precipitation revealed in water isotope ratios. *Nat. Geosci.* **2016**, *9*, 624. https://doi.org/10.1038/NGEO2739
23. Chakraborty, S.; Sinha, N.; Chattopadhyay, R.; et al. Atmospheric controls on the precipitation isotopes over the Andaman Islands, Bay of Bengal. *Sci. Rep.* **2016**, *6*, 19555. https://doi.org/10.1038/srep19555
24. Ansari, M.A.; Mohokar, H.V.; Deodhar, A.; et al. Distribution of environmental tritium in rivers, groundwater, mine water, and precipitation in Goa, India. *J. Environ. Radioact.* **2018**, *189*, 120–126. https://doi.org/10.1016/j.jenvrad.2018.04.004
25. Fousiya, A.A.; Aravind, G.H.; Achyutan, H.; et al. Modulation of the precipitation isotopes by the dynamic and thermodynamic variables of the atmosphere in southern parts of India. *Water Resour. Res.* **2022**, *58*, e2021WR030855. https://doi.org/10.1029/2021WR030855
26. Datye, A.; Chakraborty, S.; Chattopadhyay, R.; et al. Precipitation isotopes response to the atmospheric processes over the mainland and the island region in the Northern Indian Ocean: Implications to the paleo-monsoon study. *Mausam* **2023**, *74*, 503–512. https://doi.org/10.54302/mausam.v74i2.5998
27. He, X.; Kang, S.; Wang, S.; et al. Effect of below-cloud evaporation on stable isotopes in precipitation revealed by 12-year observation in the Tanggulu Mountains, Central Tibetan Plateau. *J. Hydrol.* **2025**, *663*, 134300. https://doi.org/10.1016/j.jhydrol.2025.134300
28. Rozanski, K.; Araguas, L.; Gonfiantini, R. Isotopic patterns in modern global precipitation. In *Climate Change in Continental Isotopic Records*; Swart, P.K., et al., Eds.; *Geophys. Monogr. Ser.*; American Geophysical Union: Washington, DC, USA, 1993; Volume 78, pp. 1–36.
29. Guo, X.; Tian, L.; Wen, R.; et al. Controls of precipitation δ^{18}O on the Northwestern Tibetan Plateau: A case study at Nagari station. *Atmos. Res.* **2017**, *189*, 141–151. https://doi.org/10.1016/j.atmosres.2017.02.004
30. Noble, J.; Ansari, M.A. Isotope hydrology and geophysical techniques for reviving a part of the drought prone areas of Vidarbha, Maharashtra, India. *J. Hydrol.* **2019**, *570*, 495–507. https://doi.org/10.1016/j.jhydrol.2019.01.020
31. Ansari, M.A.; Noble, J.; Deodhar, A.; et al. Stable isotopic (δ^{18}O and δ^{2}H) and geospatial approach for evaluating extreme rainfall events. *Glob. Planet. Change* **2020**, *194*, 103299. https://doi.org/10.1016/j.gloplacha.2020.103299
32. Ansari, M.A.; Noble, J.; Kumar, U.S.; et al. Assessing the groundwater recharge processes in intensively irrigated regions: An approach combining isotope hydrology and machine learning. *Geosci. Front.* **2025**, *16*, 102105. https://doi.org/10.1016/j.gsf.2025.102105
33. Zwart, C.; Munksgaard, N.C.; Kurita, N.; et al. Stable isotopic signature of Australian monsoon controlled by regional convection. *Quat. Sci. Rev.* **2016**, *151*, 228–235.
34. He, S.; Goodkin, N.F.; Jackisch, D.; et al. Continuous real-time analysis of the isotopic composition of precipitation during tropical rain events: Insight into tropical convection. *Hydrol. Process.* **2018**, *32*, 1531–1545. https://doi.org/10.1002/hyp.11520
35. Li, Y.; Zhao, C.; Deng, Q.; et al. Isotopic analysis of precipitation during rainstorm and typhoon events from the warm season in the southeastern coast of China. *J. Hydrol. Reg. Stud.* **2025**, *61*, 102749. https://doi.org/10.1016/j.ejrh.2025.102749
36. Murillo, R.S.; Quesada, A.M.D.; Hernandez, G.E.; et al. Deciphering key processes controlling rainfall isotopic variability during extreme tropical cyclones. *Nat. Commun.* **2019**, *10*, 4321. https://doi.org/10.1038/s41467-019-12062-3
37. Xu, T.; Sun, X.; Hong, H.; et al. Stable isotope ratios of typhoon rains in Fuzhou, Southeast China, during 2013–2017. *J. Hydrol.* **2019**, *570*, 445–453. https://doi.org/10.1016/j.jhydrol.2019.01.017
38. Kim, T.; Choo, S.; Moon, J.; et al. Contribution of tropical cyclones to abnormal sea surface temperature warming in the yellow sea in December 2004. *Dyn. Atmos. Oceans* **2017**, *80*, 97–109.
39. Cao, X.; Wu, R.; Wang, P.; et al. Impact of Arctic Sea ice anomalies on tropical cyclogenesis over the eastern North Pacific: Role of Northern Atlantic Sea Surface temperature anomalies. *Atmos. Res.* **2025**, *315*, 107844. https://doi.org/10.1016/j.atmosres.2024.107844
40. Palmén, E.H. On the formation and structure of tropical cyclones. *Geophysica* **1948**, *3*, 26–38.
41. Tory, K.J.; Dare, R.A. Sea surface temperature thresholds for tropical cyclone formation. *J. Clim.* **2015**, *28*, 8171–8183.
42. Arora, K.; Dash, P. Towards dependence of tropical cyclone intensity on sea surface temperature and its response in a warming world. *Climate* **2016**, *4*, 30. https://doi.org/10.3390/cli4020030
43. McTaggart-Cowan, R.; Galarneau, T.J.; Bosart, L.F.; et al. A global climatology of baroclinically influenced tropical cyclogenesis. *Mon. Weather Rev.* **2013**, *141*, 1963–1989. https://doi.org/10.1175/MWR-D-12-00186.1
44. Malkus, J.S. Cloud patterns over tropical oceans. *Science* **1963**, *141*, 767–778.
45. Evans, J.L.; Waters, J.J. Simulated relationships between sea surface temperature and tropical convection in climate models and their implications for tropical cyclone activity. *J. Clim.* **2012**, *25*, 7884–7895. https://doi.org/10.1175/JCLI-D-11-00392.1
46. Sandeep, S.F.; Stordal, J. Use of OLR data in detecting precipitation extremes in the tropics. *Remote Sens. Lett.* **2013**, *4*, 570–578. https://doi.org/10.1080/2150704X.2013.769284
47. Groning, M.; Lutz, H.O.; Roller-Lutz, Z.; et al. A simple rain collector preventing water re-evaporation dedicated for δ^{18}O and δ^{2}H analysis of cumulative precipitation samples. *J. Hydrol.* **2012**, *448–449*, 195–200.
48. Epstein, M.; Mayeda, T. Variation of δ^{18}O content in waters from natural sources. *Geochim. Cosmochim. Acta* **1953**, *4*, 213–224.
49. Craig, H. Isotopic variations in meteoric waters. *Science* **1961**, *133*, 1702–1703.
50. Clark, I.; Fritz, P. *Environmental Isotopes in Hydrogeology*; Lewis Publishers: New York, NY, USA, **1997**.
51. Liebmann, B.; Smith, C.A. Description of a complete (interpolated) outgoing longwave radiation dataset. *Bull. Am. Meteorol. Soc.* **1996**, *77*, 1275–1277.
52. Draxler, R.R.; Rolph, G.D. *HYSPLIT (Hybrid Single-Particle Lagrangian Integrated Trajectory) Model Access via NOAA ARL READY Website*. NOAA Air Resources Laboratory: Silver Spring, MD, USA, 2014. https://ready.arl.noaa.gov/HYSPLIT.php (accessed on 15 September 2025)
53. Blondi, R.; Ho, S.; Randel, W.; Tropical cyclone cloud-top height and vertical temperature structure detection using GPS radio occultation measurement. *J. Geophys. Res. Atmos.* **2013**, *118*, 5247–5259.
54. Gedzelman, S.; Lawrence, J.; Gamache, J.; et al. Probing hurricanes with stable isotopes of rain and water vapor. *Mon. Weather Rev.* **2003**, *131*, 1112–1127.
55. Fudeyasu, H.; Ichiyanagi, K.; Sugimoto, A.; et al. Isotope ratios of precipitation and water vapor observed in typhoon Shanshan. *J. Geophys. Res.* **2008**, *113*, D12113. https://doi.org/10.1029/2007JD009313
56. Lawrence, J.R.; Gedzelman, S.D.; Black, M.; et al. Stable isotopes of precipitation collected at 3 km elevation in Hurricane Olivia (1994).

J. Atmos. Chem. **2002**, *41*, 67–82.

57. Dansgaard, W. Stable isotopes in precipitation. *Tellus* **1964**, *XVI*, 436–446.
58. Zhou, J.; Li, T. A tentative study of the relationship between annual $\delta^{18}O$ & δD variations of precipitation and atmospheric circulations: A case from Southwest China. *Quat. Int.* **2018**, *479*, 117–127. https://doi.org/10.1016/j.quaint.2017.05.038
59. Pfahl, S.; Sodemann, H. What controls deuterium excess in global precipitation? *Clim. Past* **2014**, *10*, 771–781. https://doi.org/10.5194/cp-10-771-2014
60. Liu, F.; Tian, L.; Cai, Z.; et al. What caused the lag between oxygen-18 and deuterium excess in atmospheric vapour and precipitation during the earlier summer season in Southwest China? *J. Hydrol.* **2024**, *644*, 132087. https://doi.org/10.1016/j.jhydrol.2024.132087
61. Xia, Z. Quantifying the fingerprint of oceanic moisture source conditions in deuterium and 17O excess parameters of precipitation. *Geophys. Res. Lett.* **2023**, *50*, e2022GL101901. https://doi.org/10.1029/2022GL101901
62. Benetti, M.; Reverdin, G.; Pierre, C.; et al. Deuterium excess in marine water vapor: Dependency on relative humidity and surface wind speed during evaporation. *J. Geophys. Res. Atmos.* **2014**, *119*, 584–593. https://doi.org/10.1002/2013JD020535
63. Rahul, P.; Prasanna, K.; Ghosh, P.; et al. Stable isotopes in water vapor and rainwater over the Indian sector of the southern ocean and estimation of fraction of recycled moisture. *Sci. Rep.* **2018**, *8*, 7552. https://doi.org/10.1038/s41598-018-25522-5
64. Balagizi, C.M.; Marcellin, M.K.; Cuoco, E.; et al. Influence of moisture source dynamics and weather patterns on stable isotope ratios of precipitation in Central-Eastern Africa. *Sci. Total Environ.* **2018**, *628-629*, 1058–1078. https://doi.org/10.1016/j.scitotenv.2018.01.284
65. Pang, H.X.; He, Y.Q.; Zhang, Z.L.; et al. The origin of summer monsoon rainfall at New Delhi by deuterium excess. *Hydrol. Earth Syst. Sci.* **2004**, *8*, 115–118.
66. Hollins, S.E.; Hughes, C.E.; Crawford, J.; et al. Rainfall isotope variations over the Australian continent—implications for hydrology and isoscape applications. *Sci. Total Environ.* **2018**, *645*, 630–645. https://doi.org/10.1016/j.scitotenv.2018.07.082
67. Kumar, U.S.; Ansari, M.A. Environmental protection: Managing fresh water resources. In *Encyclopedia of Nuclear Energy*; Greenspan, E., Ed.; Elsevier: Netherland, 2021; Volume 4, pp. 465–484. https://doi.org/10.1016/B978-0-12-819725-7.00064-7
68. Good, S.P.; Mallia, D.V.; Lin, J.C.; et al. Stable isotope analysis of precipitation samples obtained via crowdsourcing reveals the spatiotemporal evolution of superstorm sandy. *PLoS ONE* **2014**, *9*, e91117.
69. Munksgaard, N.C.; Zwart, C.; Kurita, N.; et al. Stable isotope anatomy of tropical cyclone Ita, North-Eastern Australia, April 2014. *PLoS ONE* **2015**, *10*, e0119728. https://doi.org/10.1371/journal.pone.0119728
70. Kutty, G.; Gohil, K. The role of mid-level vortex in the intensification and weakening of tropical cyclones. *J. Earth Syst. Sci.* **2017**, *126*, 94. https://doi.org/10.1007/s1240-017-0879-y
71. Kotal, S.D.; Kundu, P.K.; Bhowmik, S.K.R. An analysis of sea surface temperature and maximum potential intensity of tropical cyclone over the bay of Bengal between 1981 and 2000. *Meteorol. Appl.* **2009**, *16*, 169–177. https://doi.org/10.1002/met.96
72. Rafiq, L.; Blaschke, T.; Tajbar, S. Arabian sea cyclone: Structure analysis using satellite data. *Adv. Space Res.* **2015**, *56*, 2235–2247.
73. Knutson, T.; Tuleya, R.; Shen, W.; et al. Impact of CO2-induced warming on hurricane intensities as simulated in a hurricane model with ocean coupling. *J. Clim.* **2001**, *14*, 2458–2468.
74. Lau, K.M.; Wu, H.T.; Bony, S. The role of large-scale atmospheric circulation in the relationship between tropical convection and sea surface temperature. *J. Clim.* **1997**, *10*, 381–392.
75. Munksgaard, N.C.; Wurster, C.M.; Bass, A.; et al. Extreme short-term stable isotope variability revealed by continuous rainwater analysis. *Hydrol. Process.* **2012**, *26*, 3630–3634. https://doi.org/10.1002/hyp.9505
76. Ansari, M.A.; Noble, J.; Deodhar, A.; et al. Isotope hydrogeochemical models for assessing the hydrological processes in a part of the largest continental flood basalts province of India. *Geosci. Front.* **2022**, *13*, 101336. https://doi.org/10.1016/j.gsf.2021.101336